Dead-Time Effect on Two-Level Voltage Source Virtual Synchronous Machines

Dead–Time Effect on Two–Level Voltage Source Virtual Synchronous Machines

Vincenzo Mallemaci
Dipartimento Energia "Galileo Ferraris"
Politecnico di Torino
Torino, 10129, Italy
vincenzo.mallemaci@polito.it

Fabio Mandrile
Dipartimento Energia "Galileo Ferraris"
Politecnico di Torino
Torino, 10129, Italy
fabio.mandrile@polito.it

Enrico Carpaneto
Dipartimento Energia "Galileo Ferraris"
Politecnico di Torino
Torino, 10129, Italy
enrico.carpaneto@polito.it

Radu Bojoi
Dipartimento Energia "Galileo Ferraris"
Politecnico di Torino
Torino, 10129, Italy
radu.bojoi@polito.it

***Abstract*—The Virtual Synchronous Machine (VSM) concept represents a valid solution to integrate renewable energy sources into the grid to provide straightforwardly grid services (e.g., inertial behavior, harmonic sink), grid support during faults and island operation. Under non–ideal (symmetric and sinusoidal) operating conditions, VSMs can behave as harmonic and unbalance sinks, improving the voltage quality at the point of connection to the grid. However, the inverter dead–time alters the harmonic and unbalance sink capability of voltage source VSMs. To demonstrate the negative influence of the dead–time effect, this paper uses a simplified method to predict the ideal behavior of voltage source VSMs under non–ideal grid voltage conditions. The paper demonstrates through experiments that: (1) the inverter dead–time effect limits the harmonic and unbalance sink capability of voltage source VSMs under non–ideal grid voltage conditions and (2) a dead–time compensation is needed to make the voltage source VSMs behave according to the theoretical analysis. Two experimental tests under a 5% grid voltage unbalance and a 10% grid voltage fifth harmonic distortion validate the negative influence of the dead–time and the beneficial effect of its compensation.**

***Index Terms*—virtual synchronous machine, grid forming, dead–time, harmonic sink, unbalance sink**

I. Introduction

According to the recent grid codes, inverter–interfaced renewable energy sources (e.g., solar and wind) will be required to provide grid services (e.g., inertial behavior, active and reactive power regulation), grid support during faults and island operation. Control algorithms based on the Virtual Synchronous Machine (VSM) concept can make power electronic converters behave as conventional synchronous machines (SMs), by providing the aforementioned grid services [1]–[3]. Moreover, VSMs can operate as harmonic and unbalance sinks, improving the voltage quality at the point of connection to the grid, i.e., the point of common coupling (PCC), through an harmonic current flow [4]–[9]. Among the several VSM models available in the literature, voltage source VSMs are wide–employed solutions to make the converter able to operate both in grid–following and grid–forming configuration [10]–[15]. Their main advantage compared to other solutions is their better capability to stably operate in case of weak grids [16], [17]. Voltage source VSMs provide the voltage reference v_i^* directly to the PWM modulator with no current loop control. However, the inverter dead–time effect introduces a non–negligible voltage error between the reference and the actual voltage provided by the converter. Nevertheless, this error does not affect the VSMs performance under normal operating conditions (i.e., symmetrical and sinusoidal) because the error is compensated by the power loop control of the VSMs. However, in case of non–ideal grid voltage conditions (i.e., voltage unbalance, harmonic distortions) the voltage error cannot be compensated because of the lack of a current loop control. Consequently, under non–ideal conditions the inverter dead–time reduces the voltage imposed by the VSMs and their harmonic current flow, thus limiting their harmonic and unbalance sink capability.

According to the authors' best knowledge, the negative influence of the switching dead–time on the harmonic and unbalance sink capability of VSMs has not been analyzed in the literature. Therefore, this paper applies a simplified method to predict the behavior of two different voltage source VSM solutions under non–ideal grid voltage conditions. The considered VSM solutions are the Osaka model [11], [12] and the VISMA II model [13]. They have been chosen because they are two of the most representative voltage source VSM models available in the literature. The results of this paper can be extended to other voltage source VSMs, such as the first version of the Synchronverter [10].

Next, experimental tests demonstrate that:

- The inverter dead–time effect limits the harmonic and unbalance sink capability of voltage source VSMs with respect to the theoretical analysis;
- A dead–time compensation is needed to make the harmonic and unbalance sink capability of voltage source

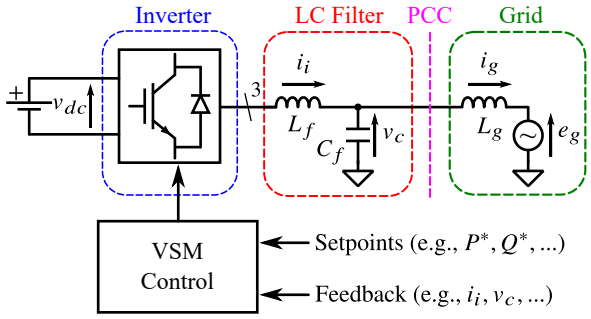

Fig. 1. Considered hardware for VSM implementations.

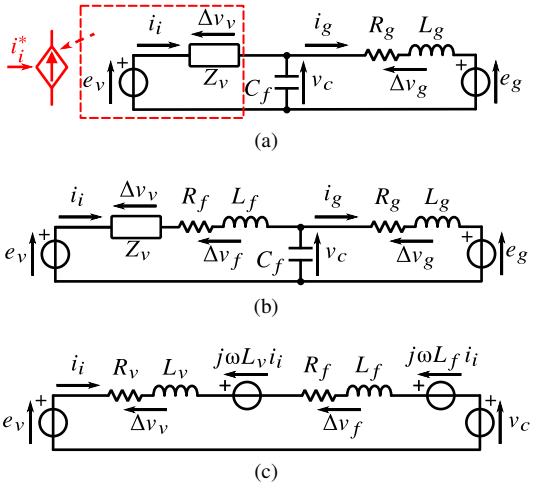

Fig. 2. (a) single phase equivalent circuit of connection between a current source VSM and the grid; (b) single phase equivalent circuit of connection between a voltage source VSM and the grid; (c) equivalent circuit in the (d, q) reference frame rotating at ω.

VSMs almost match the theoretical analysis.

The Osaka and VISMA II models have been implemented on a standard grid–tied two–level inverter, as described in Fig. 1. The experimental validation has been performed for the following testing conditions:

- Test 1: 5% of negative sequence on the grid voltage e_g, which occurs in case of asymmetrical faults;
- Test 2: 10% of fifth harmonic distortion on the grid voltage e_g, the most dominant non–fundamental component in non–ideal three phase systems.

This paper is organized as follows. Section II describes the VSM models under study and the method used to predict their behavior under non–ideal grid voltage conditions. Next, the theory of the dead–time effect and the employed dead–time compensation method are described in Section III. Section IV shows the experimental tests with and without dead–time compensation under non–ideal grid voltage conditions. Finally, Section V concludes the paper.

II. VSM Models

In general, the VSM models can be gathered into two main categories: current source and voltage source [3]. Current source VSMs include a closed loop control which tracks the

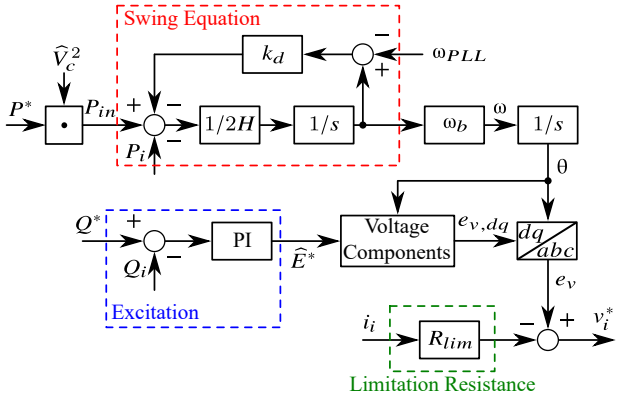

Fig. 3. Scheme of the Osaka model in the Laplace domain.

VSM current reference i_i^*. Therefore, they can be represented by the single phase equivalent circuit of connection between them and the grid depicted in Fig. 2a, where Z_v is a tunable virtual impedance, C_f is the filter capacitor of the LC filter, L_g is the grid inductance and R_g is the grid resistance.

On the other hand, voltage source VSMs do not feature a closed loop current control. Instead, these models generate a voltage reference v_i^* that is provided to the PWM modulator. This voltage reference v_i^* can be:

- Equal to the VSM electromotive force e_v, as happens for the Osaka model;
- Calculated as the difference between the VSM electromotive force e_v and the voltage drop on a tunable virtual impedance Z_v, as happens for the VISMA II model.

The focus of this paper is on voltage source models. In particular, the Osaka and VISMA II models will be considered, as representative of this category.

The scheme of the Osaka model is illustrated in Fig. 3. The swing equation is used to retrieve the VSM speed ω and the virtual angle θ. The amplitude of the virtual electromotive force $\widehat{E}^*$ is calculated by the excitation control, which consists of a PI regulator. Finally, the three phase virtual electromotive force e_v can be obtained through the Park transformation. The limitation resistance R_{lim} is used to limit the current in case of faults. For the scope of this paper R_{lim} is set to zero. The original scheme of the Osaka model embeds also the active and reactive droop control loops. As they are disabled for the purpose of this paper, they are not included in the scheme of Fig. 3. All the quantities are in per unit (pu).

The scheme of the VISMA II model is depicted in Fig. 4, showing some differences with respect to the Osaka model. Indeed, the VISMA II model employs a modified version of the swing equation written in terms of torque to retrieve the virtual speed ω and consequently the virtual angle θ. The virtual electromotive force amplitude $\widehat{E}^*$ is directly set by the user (1 pu) and used to retrieve the three phase virtual electromotive force e_v. Next, as stated before, the voltage reference v_i^* can be computed as the difference between e_v and the voltage drop on a tunable virtual impedance Z_v (which consists of a virtual resistance R_v and a virtual inductance L_v).

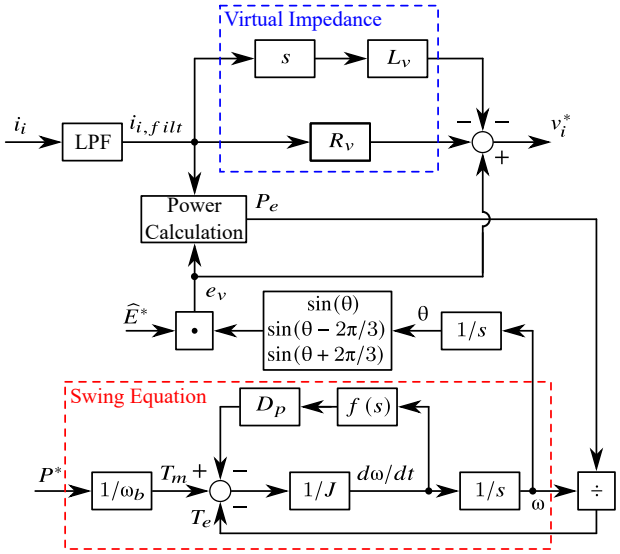

Fig. 4. Scheme of the VISMA II model in the Laplace domain.

The derivative calculus implies the use of a low pass filter (LPF) on the three phase current i_i. A complete description of the two models together with the parameter tuning procedure can be found in [3], [11]–[13].

The single phase equivalent circuit of connection between the VISMA II model and the grid is depicted in Fig. 2b, where L_f and R_f are the LC filter inductance and resistance, respectively. The other elements are the same as Fig. 2a. For the Osaka model the equivalent circuit is the same assuming a zero virtual impedance.

In the (d,q) reference frame rotating at the fundamental frequency ω, the generic quantity $\bar{x}$ can be written as follows:

$$\bar{x} = x_d + jx_q \tag{1}$$

where j is the imaginary unit, while x_d and x_q are the two components of $\bar{x}$ on the d–axis and the q–axis, respectively.

Considering the circuit in Fig. 2b, the Kirchhoff's voltage law in the (d,q) reference frame rotating at ω, is the following:

$$\bar{e}_v = (R_v + R_f)\bar{i}_i + (L_v + L_f)\frac{d\bar{i}_i}{dt} + j\omega(L_v + L_f)\bar{i}_i + \bar{v}_c \tag{2}$$

Assuming $i_i \simeq i_g$ (i.e., capacitor current negligible), for the generic harmonic h, (2) becomes:

$$\begin{aligned}\bar{e}_v^h =& (R_v + R_f)\bar{i}_i^h + j(h+1)\omega(L_v + L_f)\bar{i}_i^h + \bar{v}_c^h \\ =& \underbrace{(R_v + R_f + R_g)}_{R_{eq}}\bar{i}_i^h \\ &+ \underbrace{j\,(h+1)\omega(L_v + L_f + L_g)}_{X_{eq}^h}\bar{i}_i^h + \bar{e}_g^h \\ =& (R_{eq} + jX_{eq}^h)\bar{i}_i^h + \bar{e}_g^h\end{aligned} \tag{3}$$

The equivalent circuit is shown in Fig. 2c. The virtual electromotive force e_v is zero for each harmonic $h \neq 0$ (h = 0 for the fundamental frequency). Therefore, the harmonic current amplitude $|\bar{i}_i^h|$ can be computed as follows:

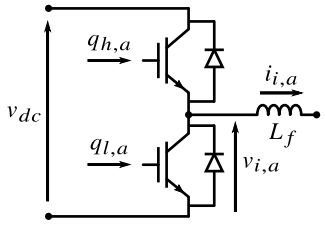

Fig. 5. Phase a leg of the inverter.

$$|\bar{i}_i^h| = \frac{|\bar{e}_g^h|}{\sqrt{R_{eq}^2 + X_{eq}^{h,2}}} \tag{4}$$

where $|\bar{e}_g^h|$ is the grid voltage amplitude of the harmonic component. In case of voltage unbalance $h = -2$, i.e., 100 Hz in the (d,q) reference frame. In case of fifth harmonic distortion $h = -6$, i.e., 300 Hz in the (d,q) reference frame.

This result is valid for the VISMA II model and also for the Osaka model assuming $R_v = 0$ and $L_v = 0$.

The main advantage of voltage source VSMs with respect to current source VSMs is their better capability to stably operate in case of weak grids [16], [17]. However, the lack of a closed loop current control leads to two main disadvantages. First, they need a backup strategy to preserve the operation of the converter even during fault conditions [3], [18]. Second, under non–ideal conditions (harmonics or unbalance), their harmonic and unbalance sink capabilities are adversely altered by the switching dead–time. The dead–time does not affect their response at the fundamental frequency as it is compensated by the active and reactive loop controls. However, for a generic harmonic $h \neq 0$, the dead–time introduces a non–compensated voltage error on the voltage reference v_i^*, which reduces the actual current drawn by the inverter with respect to the theoretical value of $|\bar{i}_i^h|$, and thus the VSM harmonic and unbalance sink performance.

III. Dead Time Effect

In a two–level inverter, a dead–time t_d between the switching commands of the switches belonging to the same leg is necessary to avoid the leg shoot through during switching operation. Fig. 5 shows the scheme of a two–level inverter leg for the phase a, where $q_{h,a}$ and $q_{l,a}$ are the switches commands for the high switch and low switch, respectively. The dead–time generation is illustrated in Fig. 6, where T_{sw} is the switching period, v_{tr} is the triangular carrier signal and v_{mod} is the modulation control voltage. The dead–time introduces a non–linear phase voltage error v_d, expressed as follows [19]:

$$v_d = \frac{4}{3}t_d f_{sw} v_{dc}\,\mathrm{sign}(i_i) \tag{5}$$

where f_{sw} is the switching frequency and $\mathrm{sign}(i_i)$ is the sign function of the three phase inverter current space vector i_i in a three phase reference frame [19].

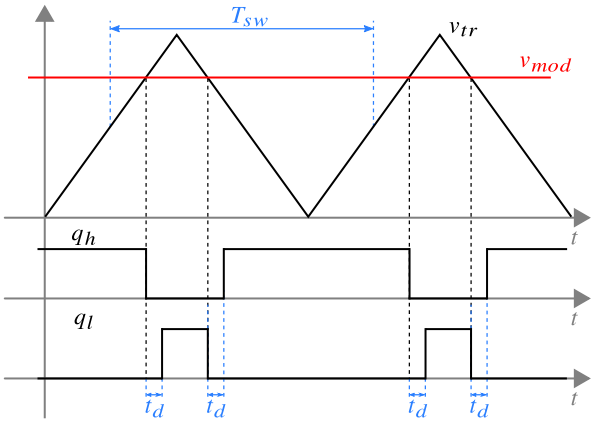

Fig. 6. Dead–time generation on the inverter control signals by the PWM technique.

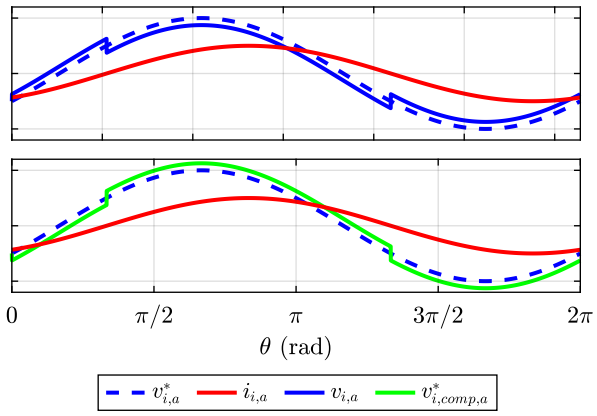

Fig. 7. Waveforms of the voltage reference v_i^*, the actual inverter current i_i, the inverter voltage moving average v_i and the compensated voltage reference $v^*_{i,comp}$ for phase a.

The dead–time effect can be observed on the output inverter voltage v_i. Fig. 7 shows the difference between the phase voltage reference $v^*_{i,a}$ and the output inverter voltage $v_{i,a}$ for phase a. As a result of the dead–time, the inverter voltage waveform is distorted. The current zero crossing determines the sign of the voltage deviation from the reference value [20]. Moreover, to better appreciate the effect of the voltage error, the sign function can be represented in the (α, β) stationary reference frame and in the (d, q) reference frame rotating at the fundamental grid frequency ω [19]. The results are shown in Fig. 8a. On the d and q axes, a voltage error whose frequency is six times the fundamental frequency is added to the mean value. These errors slightly influence the performance of VSMs at the fundamental frequency. However, under non–ideal grid voltage conditions, to counteract negative sequence distortions (e.g., voltage unbalance, fifth harmonic), the inverter current sequence is negative as well. In such conditions, the sign functions appear as illustrated in Fig. 8b for the voltage unbalance and Fig. 8c for the fifth harmonic distortion. It is evident that a non–negligible voltage error is present on both axes for these two cases. In case of voltage unbalance an error two times the fundamental frequency appears on both axes. Moreover, the error on the d–axis has a non–zero mean value. The same applies to the fifth harmonic distortion, with the difference that the error has a frequency six times the fundamental one.

As mentioned before, voltage source VSMs cannot compensate for these errors because of the lack of a closed loop current control. Therefore, the dead–time compensation must be included to guarantee their harmonic and unbalance sink capabilities. Many dead–time compensation techniques have been proposed in the literature [19]–[23]. In this paper, the adopted method refers to [20]. According to [20], the average voltage deviation ΔV, caused by the cumulative of the dead–time pulses, is computed as follows:

$$\Delta V = f_{sw} t_d v_{dc} \tag{6}$$

The deviation ΔV can be used to compensate for the dead–time by modifying the three phase voltage reference v_i^*. The compensated three phase voltage reference $v^*_{i,comp}$ can be calculated as follows:

$$v^*_{i,comp,k} = \begin{cases} v^*_{i,k} + \Delta V, & \text{if } \text{sign}(i_{i,k}) > 0^- \\ v^*_{i,k} - \Delta V, & \text{if } \text{sign}(i_{i,k}) < 0^+ \end{cases} \tag{7}$$

where k indicates the phase (i.e., a, b or c). The compensated voltage reference waveform is shown in Fig. 7 for phase a.

IV. Experimental Tests

The experimental setup is illustrated in Fig. 9. A three phase, two–level inverter is connected to a grid emulator through an LC filter. The grid emulator imposes the three phase voltage e_g. The main data are collected in Table I. Base values have been defined to express most of the parameters in per unit. The two VSM models have the same design parameters (e.g, virtual inertia, damping coefficient, etc.) as in [3].

Two experimental tests have been carried out to validate the negative dead–time influence on the harmonic sink capability of VSMs and the beneficial effect of the dead–time compensation:

- Test 1: grid voltage e_g with 5% of negative sequence. The grid voltage can contain negative sequence, for instance, in case of asymmetrical faults;
- Test 2: grid voltage e_g with 10% of fifth harmonic distortion. In three phase systems, the fifth harmonic is typically generated by non–linear loads and it is the most dominant non–fundamental harmonic component.

The values chosen for the tests are arbitrary and sufficient to appreciate the effect of the dead–time and its compensation.

A. Test 1: 5% of voltage unbalance

Considering (4), the theoretical current peaks for Osaka and VISMA II are 20.12 A and 6.82 A, respectively. The results of the test are shown in Fig. 10 and summarized in Table II. In the first 100 ms the dead–time compensation is disabled. It is evident that the current amplitudes are much lower than the expected values (1.77 A against the expected 20.12 A for

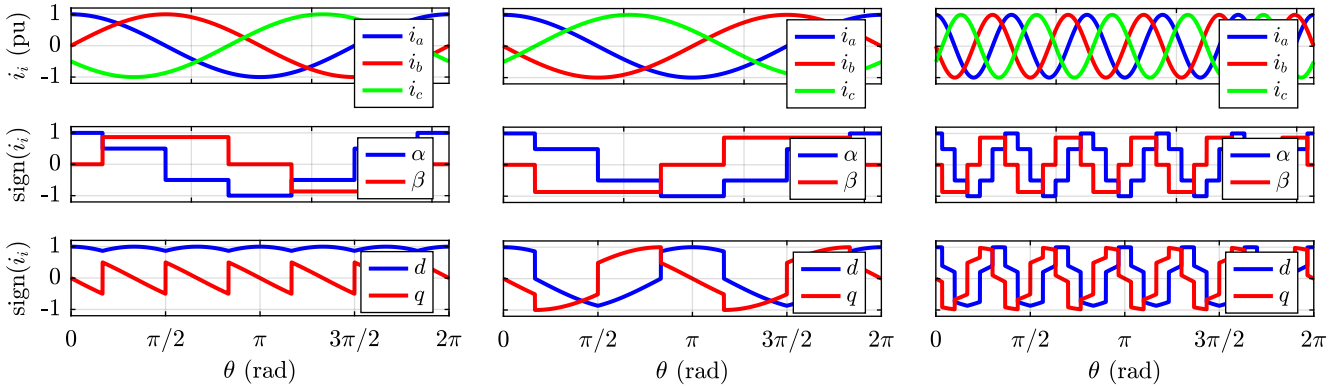

(a) (b) (c)

Fig. 8. From left to right: (a) direct sequence; (b) negative sequence; (c) fifth harmonic distortion. From top to bottom: three phase current i_i; sign(i_i) in the (α, β) reference frame; sign(i_i) in the (d, q) reference frame rotating at the fundamental frequency.

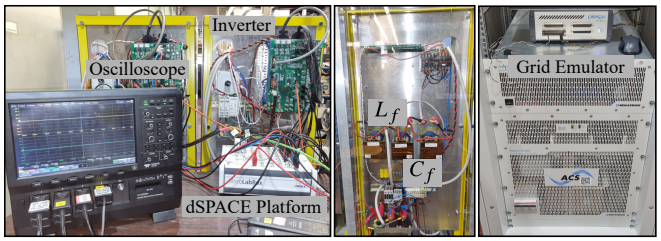

Fig. 9. Picture of the experimental setup.

TABLE I
EXPERIMENTAL SETUP AND VSM PARAMETERS.

Inverter		**Base Values**			
S_N	15 kVA	S_b	15 kVA	f_b	50 Hz
I_N	30 A	V_b	$230\sqrt{2}$ V	ω_b	314 rad/s
V_{dc}	650 V	I_b	30 A	L_b	33.7 mH
f_{sw}	10 kHz	Z_b	10.6 Ω	C_b	0.3 mF
t_d	3 µs				
Virtual Impedance		**LC Filter**		**Grid**	
R_v	0.02 pu	R_f	0.024 pu	$\widehat{E}_g$	$230\sqrt{2}$ V
L_v	0.15 pu	L_f	0.059 pu	R_g	0.009 pu
		C_f	0.017 pu	L_g	0.01 pu

Osaka and 1.62 A against the expected 6.82 A for VISMA II). Then, the dead–time compensation is enabled. After a transient, the current amplitudes reach the values of 19.88 A for Osaka and 6.62 A for VISMA II (against the expected 20.12 A and 6.82 A, respectively). They almost match the theoretical values, demonstrating the validity of both the simplified modeling method and the dead–time compensation.

B. Test 2: 10% of fifth harmonic distortion

The results of the test are illustrated in Fig. 11 and Table II. As in the previous test, in the first 100 ms the dead–time compensation is disabled. The current amplitudes are lower than the theoretical values calculated by (4): 4.61 A against 8.86 A and 1.73 A against 2.80 A, respectively for Osaka and VISMA II. Then, the dead–time compensation is enabled and also in this case the current peak values almost match the

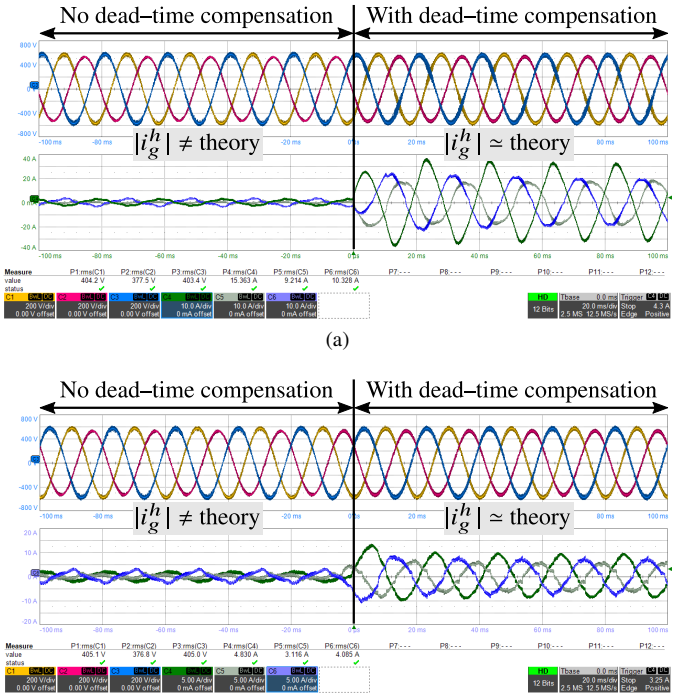

(a)

(b)

Fig. 10. PCC measured line to line voltage $v_{c,ll}$ (C1, C2, C3) and grid measured current i_g (C4, C5, C6) without and with dead–time compensation under a 5% grid voltage unbalance: (a) Osaka; (b) VISMA II.

theoretical ones (8.48 A against 8.86 A for Osaka and 2.66 A against 2.80 A for VISMA II).

V. CONCLUSION

Grid–connected converters controlled as VSMs can enhance the voltage quality at the point of connection to the grid through an harmonic current flow, by behaving as harmonic and unbalance sinks. This paper highlights the limitation of the voltage source VSMs performance caused by the switching dead–time. Two voltage source VSM models available in the literature (i.e., Osaka and VISMA II) are tested against a 5%

TABLE II
RESULTS OF THE EXPERIMENTAL TESTS.

VSM	Test	$\lvert\bar{i}_i^h\rvert$ (A) No Comp.	Comp.	Theoretical
Osaka	1	1.77	19.88	20.12
	2	4.61	8.48	8.86
VISMA II	1	1.62	6.62	6.82
	2	1.73	2.66	2.80

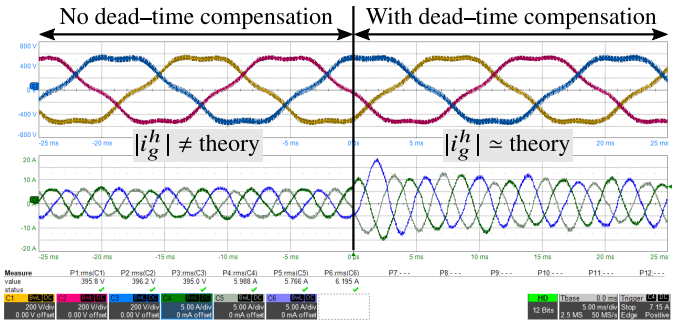

(a)

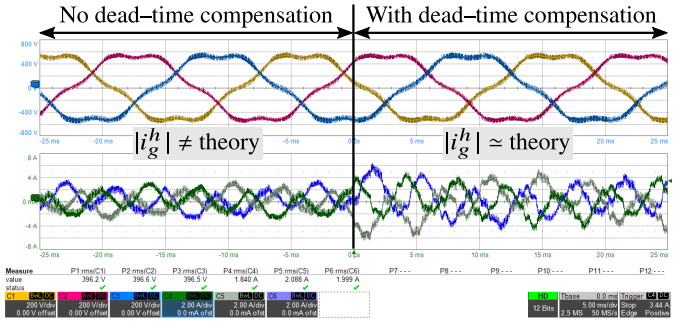

(b)

Fig. 11. PCC measured line to line voltage $v_{c,ll}$ (C1, C2, C3) and grid measured current i_g (C4, C5, C6) without and with dead–time compensation under a 10% grid voltage fifth harmonic distortion: (a) Osaka; (b) VISMA II.

of voltage unbalance and a 10% of fifth harmonic distortion. With no dead–time compensation, the injected current is much lower than the expected one, thus limiting the harmonic and unbalance sink capabilities of the VSMs. Thanks to the dead–time compensation, the experimental results almost match the theoretical behavior expected by the simplified prediction method. Therefore, this paper demonstrates the need to compensate for the switching dead–time to guarantee the harmonic and unbalance sink capability of voltage source VSMs.

REFERENCES

[1] U. Tamrakar, D. Shrestha, M. Maharjan, B. P. Bhattarai, T. M. Hansen, and R. Tonkoski, "Virtual Inertia: Current Trends and Future Directions," *Applied Sciences*, vol. 7, no. 7, p. 654, Jul. 2017.

[2] M. Chen, D. Zhou, and F. Blaabjerg, "Modelling, Implementation, and Assessment of Virtual Synchronous Generator in Power Systems," *Journal of Modern Power Systems and Clean Energy*, vol. 8, no. 3, pp. 399–411, May 2020.

[3] V. Mallemaci, F. Mandrile, S. Rubino, A. Mazza, E. Carpaneto, and R. Bojoi, "A comprehensive comparison of Virtual Synchronous Generators with focus on virtual inertia and frequency regulation," *Electric Power Systems Research*, vol. 201, p. 107516, Dec. 2021.

[4] ENTSO-E, "High Penetration of Power Electronic Interfaced Power Sources and the Potential Contribution of Grid Forming Converters," Technical Report, Jan. 2020.

[5] A. Tarrasó, J. I. Candela, J. Rocabert, and P. Rodriguez, "Grid voltage harmonic damping method for spc based power converters with multiple virtual admittance control," in *2017 IEEE Energy Conversion Congress and Exposition (ECCE)*, 2017, pp. 64–68.

[6] L. Zhou, Z. Shuai, Y. Chen, W. Wu, X. Zhou, K. Yan, and A. Luo, "Impedance-Based Harmonic Current Suppression Method for VSG Connected to Distorted Grid," *IEEE Transactions on Industrial Electronics*, vol. 67, no. 7, pp. 5490–5502, Jul. 2020.

[7] E. Avdiaj, J. Are Suul, S. D'Arco, and L. Piegari, "A Current Controlled Virtual Synchronous Machine Adapted for Operation under Unbalanced Conditions," in *2020 9th International Conference on Renewable Energy Research and Application (ICRERA)*, Sep. 2020, pp. 263–270, iSSN: 2572-6013.

[8] G. Lou, Q. Yang, W. Gu, X. Quan, J. M. Guerrero, and S. Li, "Analysis and Design of Hybrid Harmonic Suppression Scheme for VSG Considering Nonlinear Loads and Distorted Grid," *IEEE Transactions on Energy Conversion*, vol. 36, no. 4, pp. 3096–3107, Dec. 2021.

[9] T. S. Amorim, D. Carletti, and L. F. Encarnação, "Comparison of inverter controllers with synthetic inertia and harmonic compensation features," *Electric Power Systems Research*, vol. 197, p. 107344, Aug. 2021.

[10] Q. Zhong and G. Weiss, "Static synchronous generators for distributed generation and renewable energy," in *2009 IEEE/PES Power Systems Conference and Exposition*, 2009, pp. 1–6.

[11] K. Sakimoto, Y. Miura, and T. Ise, "Stabilization of a power system with a distributed generator by a virtual synchronous generator function," in *8th International Conference on Power Electronics - ECCE Asia*, 2011, pp. 1498–1505.

[12] Jia Liu, Y. Miura, and T. Ise, "Dynamic characteristics and stability comparisons between virtual synchronous generator and droop control in inverter-based distributed generators," in *2014 International Power Electronics Conference (IPEC-Hiroshima 2014 - ECCE ASIA)*, 2014, pp. 1536–1543.

[13] Y. P. Chen, R. Hesse, D. Turschner, and H.-P. Beck, "Comparison of methods for implementing virtual synchronous machine on inverters," *Renewable energy & power quality journal*, pp. 734–739, 2012.

[14] R. Rosso, X. Wang, M. Liserre, X. Lu, and S. Engelken, "Grid-Forming Converters: Control Approaches, Grid-Synchronization, and Future Trends—A Review," *IEEE Open Journal of Industry Applications*, vol. 2, pp. 93–109, 2021.

[15] C. Li, Y. Yang, Y. Cao, L. Wang, and F. Blaabjerg, "Frequency and Voltage Stability Analysis of Grid-Forming Virtual Synchronous Generator Attached to Weak Grid," *IEEE Journal of Emerging and Selected Topics in Power Electronics*, vol. 10, no. 3, pp. 2662–2671, Jun. 2022.

[16] W. Wu, Y. Chen, L. Zhou, A. Luo, X. Zhou, Z. He, L. Yang, Z. Xie, J. Liu, and M. Zhang, "Sequence impedance modeling and stability comparative analysis of voltage-controlled vsgs and current-controlled vsgs," *IEEE Transactions on Industrial Electronics*, vol. 66, no. 8, pp. 6460–6472, 2019.

[17] R. Rosso, J. Cassoli, G. Buticchi, S. Engelken, and M. Liserre, "Robust Stability Analysis of LCL Filter Based Synchronverter Under Different Grid Conditions," *IEEE Transactions on Power Electronics*, vol. 34, no. 6, pp. 5842–5853, Jun. 2019.

[18] R. Rosso, S. Engelken, and M. Liserre, "On The Implementation of an FRT Strategy for Grid-Forming Converters Under Symmetrical and Asymmetrical Grid Faults," *IEEE Transactions on Industry Applications*, vol. 57, no. 5, pp. 4385–4397, Sep. 2021.

[19] S. Bolognani and M. Zigliotto, "Self-commissioning compensation of inverter non-idealities for sensorless AC drives applications," in *2002 International Conference on Power Electronics, Machines and Drives (Conf. Publ. No. 487)*, Jun. 2002, pp. 30–37, iSSN: 0537-9989.

[20] L. Ben-Brahim, "The analysis and compensation of dead-time effects in three phase PWM inverters," in *IECON '98. Proceedings of the 24th Annual Conference of the IEEE Industrial Electronics Society (Cat. No.98CH36200)*, vol. 2, Aug. 1998, pp. 792–797 vol.2.

[21] A. Munoz and T. Lipo, "On-line dead-time compensation technique for open-loop PWM-VSI drives," *IEEE Transactions on Power Electronics*, vol. 14, no. 4, pp. 683–689, Jul. 1999.

[22] N. Urasaki, T. Senjyu, K. Uezato, and T. Funabashi, "An adaptive dead-time compensation strategy for voltage source inverter fed motor drives,"

IEEE Transactions on Power Electronics, vol. 20, no. 5, pp. 1150–1160, Sep. 2005.

[23] G. Pellegrino, P. Guglielmi, E. Armando, and R. I. Bojoi, "Self-Commissioning Algorithm for Inverter Nonlinearity Compensation in Sensorless Induction Motor Drives," *IEEE Transactions on Industry Applications*, vol. 46, no. 4, pp. 1416–1424, Jul. 2010.